IEEE Photonics Journal
An IEEE Photonics Society Publication

Open Access

Design for a Single-Polarization Photonic Crystal Fiber Wavelength Splitter Based on Hybrid-Surface Plasmon Resonance

Volume 6, Number 4, August 2014

Lei Chen
Weigang Zhang
Zhao Zhang
Yongji Liu
Jonathan Sieg
Liyu Zhang
Quan Zhou
Li Wang
Biao Wang
Tieyi Yan

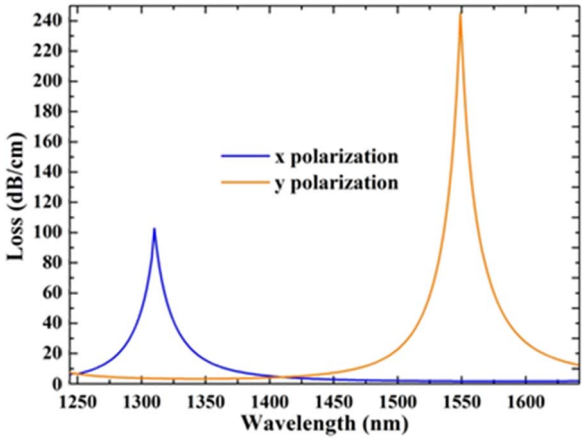

DOI: 10.1109/JPHOT.2014.2331237
1943-0655

Design for a Single-Polarization Photonic Crystal Fiber Wavelength Splitter Based on Hybrid-Surface Plasmon Resonance

Lei Chen, Weigang Zhang, Zhao Zhang, Yongji Liu, Jonathan Sieg, Liyu Zhang, Quan Zhou, Li Wang, Biao Wang, and Tieyi Yan

Key Laboratory of Opto-electronic Information Science and Technology, Ministry of Education, Institute of Modern Optics, College of Information Technical Science, Nankai University, Tianjin 300071, China

DOI: 10.1109/JPHOT.2014.2331237

Manuscript received May 19, 2014; revised June 8, 2014; accepted June 12, 2014. Date of publication June 17, 2014; date of current version June 27, 2014. This work was supported in part by the National Natural Science Foundation under Grants 11274181, 10974100, 10674075, and 11104149, by the Doctoral Scientific Fund Project of the Ministry of Education under Grant 20120031110033, and by the Tianjin Key Program of Application Foundations and Future Technology Research Project under Grant 10JCZDJC24300. Corresponding author: W. G. Zhang (e-mail: zhangwg@nankai.edu.cn).

Abstract: A novel single-polarization photonic crystal fiber wavelength splitter based on hybrid-surface plasmon resonance is proposed. A full-vector finite-element method is applied to analyze the guiding properties. Numerical simulations show that the proposed splitter, which is only several hundred microns in length, gives single polarization in the 1.31-μm and 1.55-μm bands. The loss of the unwanted polarized mode is 102.6 and 245.0 dB/cm in the two aforementioned communication windows, respectively, and the corresponding insertion loss is as low as 3.5 and 1.7 dB/cm, respectively. Moreover, the dependence of the bandwidth on the fiber length is given, and according to that function, the bandwidth can reach 40 nm (1.31-μm band) and 100 nm (1.55-μm band) when the fiber length is up to 1 mm. Additionally, the tolerances for a realistic fabrication are analyzed. In the last part, we discuss other methods to deal with an anticrossing phenomenon in detail.

Index Terms: Fiber design, surface plasmons, photonic crystal fibers.

1. Introduction

The wavelength division multiplexer (WDM) is a key component in modern optoelectronic and communication systems, especially for the area of passive optical networks. Due to the silica-based fiber consisting of a backbone or access net and the relatively low propagation loss in the nature of silica in the wavelength bands of 1.31 μm and 1.55 μm, the WDM served for these bands has been used for carrying data in practical applications. Consequently, its counterpart—a demodulator serving for the aforementioned communication windows has been fabricated and continues to upgrade along with the rapid development of wavelength division multiplexing technology. Since photonic crystal fibers (PCF) were first proposed in the early 90's, many functional devices based on PCF, including modulators, multiplexers, rotators and demodulators, serving for the mentioned bands have been proposed because they provide extra freedom in controlling the propagation of light inside of them in comparison to the conventional fibers. Meanwhile, the control of polarization, such as polarization modulators [1], [2],

polarization switches [3], [4], polarization rotators [5]–[7] and polarization division multiplexing [8], becomes a new trend in communication systems and integrated optical circuits. Therefore, it is essential to propose a novel and compact device combining the wavelength splitter and the polarization.

Based on the above considerations, we recently proposed three silica-based PCF single-polarization wavelength splitters (SPWS) [9]–[11], which could suppress polarization mode coupling (PMC) and polarization mode dispersion (PMD) due to their single-polarization guiding characteristics in cores. Recently, Xue *et al.* numerically investigated the polarization of a PCF by selectively coating a metal ring and filling it with liquid [12], and the function of a polarization filter was achieved at 1.31 μm band. Du *et al.* also reported a PCF-based SPWS, which covers two communication bands based on a core mode coupling with an SP mode [13]. Li *et al.* stimulated a dual-core PCF serving for SPWS based on surface plasmon resonance and mode coupling [14]. However, all the previous wavelength splitters possess three major limitations. The first limitation is that these structures based on the beat frequency principle require accurate fiber cleaving according to the designed coupling length [9], [14], which is extremely hard when the fiber length is compact. The second limitation is that the length of the fibers of the centimeter order (silica based) is inconvenient for the compact design nowadays [10], [11]. Thirdly, the coupling between core mode and SP mode is incomplete, which has a low loss (about 50 dB/cm [13]) for the unwanted polarization compared with the couple between HSP and core mode [16]–[18].

To overcome the three aforementioned limitations and further develop a more compact SPWS, in this paper, to the best of the authors' knowledge, we design the first PCF SPWS with orthogonal polarization states based on the couple between HSP and core mode, which works for 1.31 μm and 1.55 μm bands. We use the full-vector finite-element method (FEM) to analyze the proposed device. The proposed SPWS, which is only several hundred microns in length, gives single polarization in the two communication windows and does not require a precisely matching fiber length. The loss of unwanted polarization mode can reach 102.6 dB/cm and 245.0 dB/cm in the two bands respectively and the corresponding insertion loss is only down to 3.5 dB/cm and 1.7 dB/cm. Moreover, the relation between the bandwidth and the fiber length is derived and explained. According to this relation, the bandwidth can reach 40 nm (1.31 μm band) and 100 nm (1.55 μm band) when the fiber length is up to 1 mm. In addition, the tolerances for realistic fabrication are analyzed. In the last part, we exhibit our method in dealing with the coupling between core mode and HSP mode in the PCF and review other methods in dealing with this phenomenon in detail.

2. The Principle of the Proposed SPWS and Its Structure

Surface plasmon-polaritons (SPs) form at metal-dielectric interfaces because the free electrons in the metal introduce an additional phase change upon reflection, inducing high intensity surface plasmon (SP) modes [12]–[15] or hybrid surface plasmon (HSP) modes [5], [16]–[22]. As a result, light can be confined in a space that is sub-wavelength in scale in the surrounding dielectric, leading to field enhancements. Unfortunately, SPs were not considered viable for photonic elements because of the large propagation loss by the metal in the past several years. However, the recent research results of extraordinary optical transmission (EOT) [23], [24] and HSP mode [5], [16]–[22] show that the propagation loss can be significantly reduced. Such developments make SPs possible to integrate into many SPs-based devices into photonic integrated circuits (PICs).

A hybrid plasmon waveguide (HPW), composed of a metal cap, a thin low refractive index dielectric layer and a high refractive index dielectric layer, is usually utilized within PICs. Modes propagating in the HPW can be considered a combination of SP modes at the metal/low refractive index interface and the traditional photonic guided modes in high refractive index waveguide. Therefore, they have outstanding properties of both low propagation losses and strong confinement. The explanation of HPW is very similar to that of EOT [23], [24]. However, as the

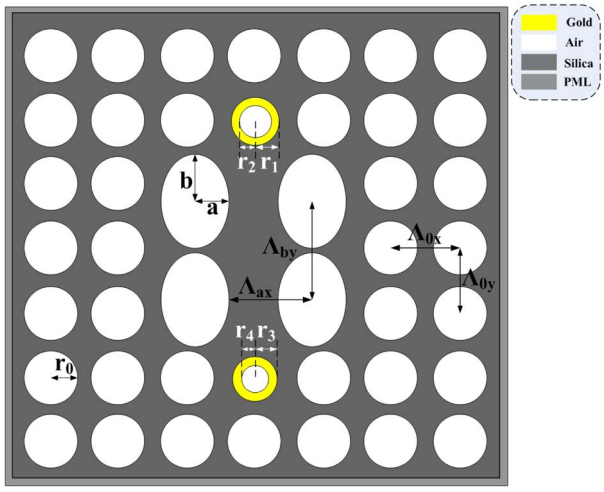

Fig. 1. Cross-section of the proposed PCF SPWS.

TABLE 1
Optimized value in the simulation

r_0 (μm)	r_1 (μm)	r_2 (μm)	r_3 (μm)	r_4 (μm)	a (μm)	b (μm)	Λ_{ax} (μm)	Λ_{by} (μm)	Λ_{0x} (μm)	Λ_{0y} (μm)
1.00	0.75	0.30	0.37	0.46	1.45	1.90	4.10	3.90	2.50	2.50

counterpart of PICs in the backbone or access, PCF HSP-based SPWS has never been specifically proposed. When a circular metallic wire or ring is embedded in silica glass, the wire or ring is intrinsically symmetric about its axis. The guided mode in the interface of the metal and silica spreads out more and more into the dielectric as the mode approaches the cut-off [25]. Consequently, the HSP mode might be expected and supported by the PCF. Although an SP mode naturally causes a greater loss than an HSP mode, the latter is better suited than the former in forming mode resonance because it matches better with the imaginary part of mode effective refractive index with a leaky mode guided in the PCF silica core. The coupled mode theory can be utilized for explaining that reason and more detailed explanations will be given with the specific structure in part 3.2.

The cross-section of the proposed PCF SPWS is shown in Fig. 1. "r_0"-"r_4" represent the radius of the background air hole, the upper hole coated by Au, the air channel in the upper Au layer, the lower hole coated Au, and the air channel in the lower Au layer, respectively. Four ellipses are arranged in the centre of the PCF lattice, which is beneficial for producing the birefringence and the letters "a" and "b" are the semi-minor axis and semi-major axis of the ellipse. $\wedge_{ax}$, $\wedge_{by}$, $\wedge_{0x}$, and $\wedge_{0y}$ are the hole pitches of the ellipse air hold and background air hole in the *x*- and *y*-axes, respectively. The different colors stand for different materials, which are shown in the legend of Fig. 1. Finally, a perfectly matched layer (PML) is used to match the outmost layer.

The background material is pure silica and its material dispersion is determined by the Sellmeier equation, in which optical constants are based on experimental results [26]. For accurate calculation, the material dispersion of Au is determined by the Drude-Lorentz model and its optical constants are based on empirical results [27]. The modal loss (defined in decibels per meter) can be defined as

$$\alpha = 40\pi \mathrm{Im}(n_{eff})/(\ln(10)\lambda)) \quad (1)$$

where λ is the optical wavelength, and $\mathrm{Im}(n_{eff})$ is the imaginary part of the effective modal refractive index. The optimized values of the parameters in the simulation are presented in Table 1.

3. Number Results and Analysis

3.1. The Dispersion Curves Characteristics of Two Au Rings

In this section, we investigate the mode dispersion properties of two aligned Au rings, but the rings' inner radii equals 0, i.e., Au wires. Two Au wires are arranged to be aligned with the same radii $(1.5\ \mu\mathrm{m} + 1.5\ \mu\mathrm{m})$ and different radii $(1.2\ \mu\mathrm{m} + 1.5\ \mu\mathrm{m})$ embedded in the silica, and in order to make a comparison we plot dispersion curves of a single Au wire with radii of 1.2 μm and 1.5 μm, respectively. For the sake of clarity, we only use 2nd SP/HSP mode as an example in the simulations.

We know the SPs will stimulate the discrete SP/HSP modes at the interface of the metal and dielectric [19], [28], and each mode processes its own polarization, for example, 2nd SP/HSP modes have two polarizations. Fig. 2(a) plots two 2nd SP modes of one Au wire with a radius of 1.5 μm embedded in silica and four 2nd SP modes of two aligned Au wires with a radius of 1.5 μm embedded in silica. The Poynting vector distributions of 2nd SP modes stimulated on the surfaces of the two structures are shown. Based on Fig. 2(a), we notice that an intriguing feature of the original degenerated 2nd SP modes is that L_2nd (1) and L_2nd (2) interact with each other, forming four new SP/HSP modes, i.e., Modes 1$\sim$4, of which the dispersion curves are shown in Fig. 2(a). In contrast, if two Au wires with different radii are aligned, their original degenerated two SP modes will split into four curves around their original dispersion curves. In addition, it is noticed that two sets of curves detune with each other, and almost keep their own original dispersion curves. Fig. 2(b) demonstrates this phenomenon. An Au wire with a radius of 1.2 μm is embedded in the silica, and its 2nd SP modes are named S_2nd (1) and S_2nd (2), and their dispersion curves are shown in Fig. 2(b). In contrast, the mode dispersion curves, i.e., Modes 5 $\sim$ 8, which are formed by the two different radii Au wires, are very similar with the single Au wire's 2nd SP mode also shown in Fig. 2(b).

Based on the analysis mentioned above, we know that two Au wires will interact with each other and form more modes, just like the case in Fig. 2(a). However, the resonance phenomenon can be avoided effectively when the difference of the radii of the Au wires is large enough, just like the case in Fig. 2(b). Therefore, based on this principle, we can remove an unwanted polarization in the different wavelength, such as the single polarization for 1.31 μm and 1.55 μm bands, by embedding different radii of Au wires/rings in the silica.

3.2. The Simulation Results of SPWS PCF and Discussion

For two coupled modes, the coupled-mode equations can be described as [29]:

$$\begin{cases} \frac{dE_1}{dz} = i\beta_1 E_1 + i\kappa E_2 \\ \frac{dE_2}{dz} = i\kappa E_1 + i\beta_2 E_2 \end{cases} \tag{2}$$

where E_1 and E_2 stand for the mode fields of leaky mode and HSP mode respectively, β_1 and β_2 are their propagation constant, and κ is the coupling strength. Assume that $E_1 = \mathrm{A}\times\ \exp(\mathrm{i}\beta\mathrm{z})$ and $E_2 = \mathrm{B} \times \exp(\mathrm{i}\beta\mathrm{z})$. The propagation constant of coupling mode, β, can be obtained by solving

$$\beta_{\pm} = \beta_{ave} \pm \sqrt{\delta^2 + \kappa^2} \tag{3}$$

where $\beta_{ave} = (\beta_1 + \beta_2)/2$, and $\delta = (\beta_1 - \beta_2)/2$. For leaky mode and HSP mode, β_1 and β_2 are both complex. So δ is also complex and can be written as $\delta = \delta_\mathrm{r} + \mathrm{i}\delta_\mathrm{i}$. At phase matching point, the real parts of the two coupled mode propagation constants are equal, i.e., $\delta_\mathrm{r} = 0$. It can be

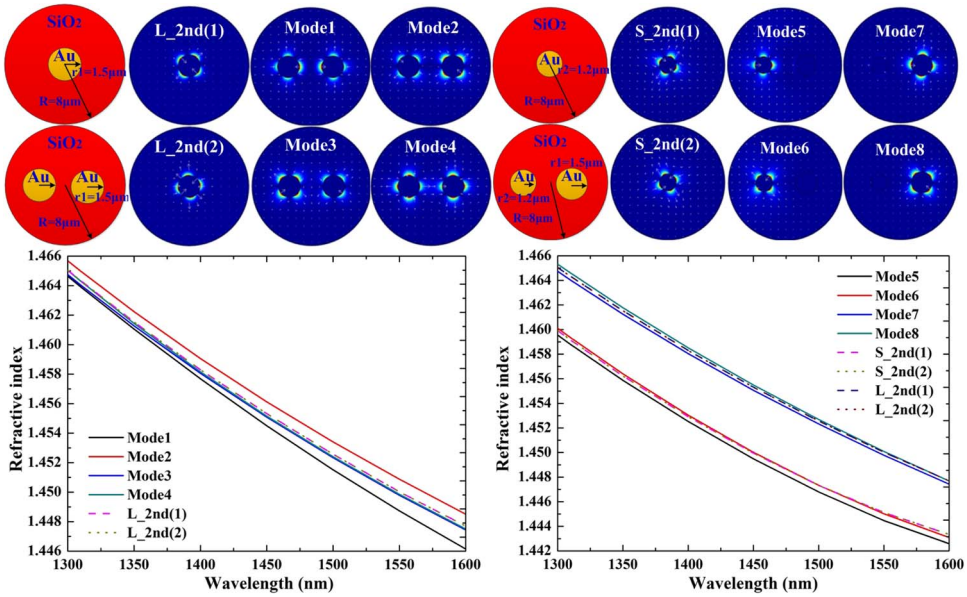

Fig. 2. Wavelength dependence on second SP/HSP mode effective refractive indices for (a) Au wires with the same radius (1.5 μm) and (b) Au wires with different radii (1.2 μm and 1.5 μm).

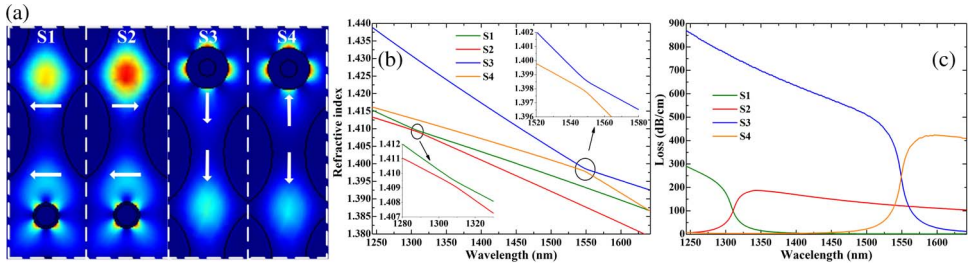

Fig. 3. Four hybridized modes and their dispersion and loss curves. (a) Modal field, (b) dispersion curves (insets are the magnification of two anti-crossing points), (c) loss curves.

derived that $\delta^2 + \kappa^2 = -\delta_i^2 + \kappa^2$. When $\delta_i < \kappa$, then β_+ and β_- possess different real parts but equal imaginary parts. A complete coupling (regular anti-crossing) between a leaky mode and an HSP mode occurs. On the contrary, the incomplete coupling happened when $\delta_i > \kappa$, β_+ and β_- have different imaginary parts but equal real parts [25].

For the sake of clarity, we only exhibit four super modes leading to the anti-crossing phenomenon. It is noticeable that the original second HSP mode and guided fundamental core mode are mixed together and formed four new hybridized modes. The only difference is the phase of the two parts in the hybridized modes. The hybridized modes are usually named odd- and even-mode [14], but the proposed SWPS has two wavelengths needed to be processed; thus for convenience we name the four modes S1, S2, S3, and S4 respectively. Based on Fig. 3(a), S1, S2, S3, and S4 have the same *x*- and *y*-axis electric field in the core section. According to the transmission line theory, the electromagnetic (EM) wave will select the medium possessing lower transmission loss. Consequently, although the concept of the original defective fundamental core mode is no longer at play, we still can call the orthogonal polarization states *x*- and *y*-polarization in terms of output and their loss curves are shown in Fig. 4. Based on Fig. 4, we can see that the loss of unwanted polarization mode can reach 102.6 dB/cm and 245.0 dB/cm in the two communication windows respectively and corresponding insertion loss is only down to 3.5 dB/cm and 1.7 dB/cm.

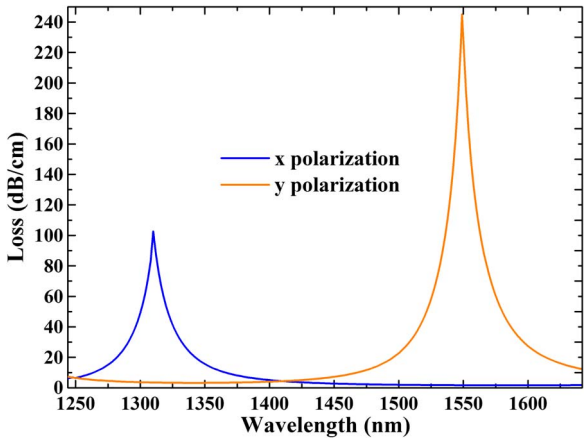

Fig. 4. Wavelength dependence of losses of the *x*- and *y*-polarization modes in the proposed PCF SWPS.

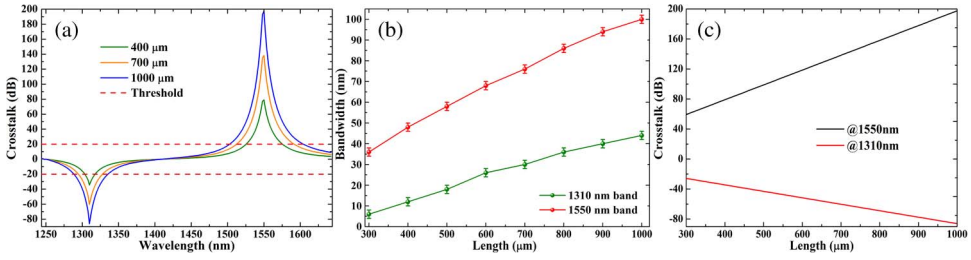

Fig. 5. Crosstalk of the proposed PCF SPWS. (a) Variation of crosstalk for different fiber length. (b) Bandwidth dependent on fiber length. (c) Crosstalk at 1310 nm and 1550 nm dependent on fiber length.

In addition, crosstalk (CT) is a key parameter for SPWS. It determines the influence of unwanted polarization modes and thus can characterize the transmission performances. According to Beer Laws [30] and the concept of CT [6], [9]–[11], the CT dependant on fiber length can be derived as

$$\mathrm{CT} = 20\lg\{\exp[(\alpha_2 - \alpha_1)L]\}$$

where α_1 and α_2 represent the loss of *x*- and *y*-polarization respectively, and *L* stands for fiber length. The results of the dependence of CT on the wavelength with different fiber length are shown in Fig. 5(a). Since the wanted polarization in the 1.31 μm band is unwanted polarization in the 1.55 μm band, the crosstalk is greater than 0 dB in the 1.55 μm band. As a result, we consider the available optical bandwidth defined as the wavelength range within which the transmission is lower than -20 dB or higher than 20 dB. The bandwidth of two bands increases with the fiber length and it can reach 40 nm in 1.31 μm band and 100 nm in 1.55 μm band when the fiber length equals 1 mm as shown in Fig. 5(b). In the simulation, dispersion curves are calculated ranging from 1250 nm to 1650 nm in steps of 2 nm, therefore the simulation error, shown as error bar in Fig. 5(b), is 2 nm, the value of which is a tradeoff between time and accuracy. Fig. 5(c) exhibits the evolution of dips and peaks in Fig. 5(a) on fiber length. Although the trends of the two curves look to be opposite, their physical meaning is the same, i.e., the crosstalk improves as the fiber length increases.

The tolerances for realistic fabrication should be analyzed for integrity. We calculated the impact of the slight changes in size of Au rings on the output spectrum. Numerical simulations reveal that the proposed device possesses a relatively strong realistic fabrication tolerance. As

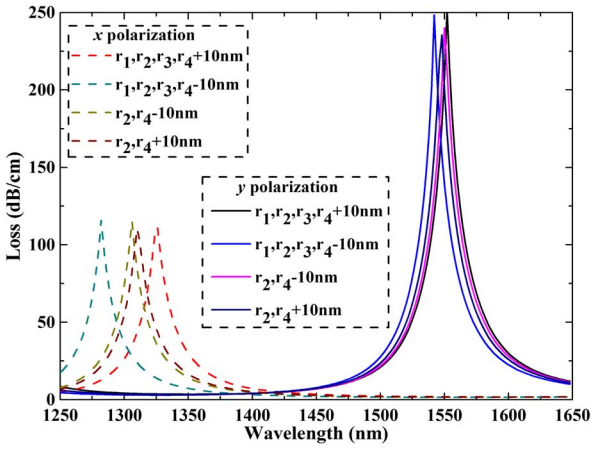

Fig. 6. Wavelength dependence of the four typical modal loss for deformation.

shown in Fig. 6, when $r_1 - r_4$ values fluctuate 10 nm, the device performance will be slightly affected. We observed that the impact of r_2 and r_4 is lower than that of r_1 and r_3, because modal loss is caused by the outside ring SP mode rather than the inside ring SP mode, and the thickness of the Au rings are thick enough, which means the evanescent wave of outside ring SP mode only has a little impact on the device spectrum. Based on Fig. 6, the third and forth curves of *x*- and *y*-polarization demonstrate our theoretical prediction, i.e., the sizes of r_2 and r_4 possess a slight impact on the output spectrum. In addition, we maintain the thickness of the Au rings, and increase and decrease the sizes of r_1 and r_3 for the sake of investigating the effects of size on the output characteristics. From Fig. 6, the first and second curves of *x*- and *y*-polarization show that the fluctuation of r_1 and r_3 has a relatively large effect on the output spectrum. Also, another phenomenon that can be found is that the dip shifting in the 1310 nm band is greater than that of the 1550 nm band, because the size of r_1 and r_2 is larger than r_3 and r_4, and 10 nm is relatively large for the small size.

In the last part, it is worth pointing out that the method with which we are dealing with the phenomenon of anti-crossing point is different than that of others. Many academic papers observe this same phenomenon but employ three different methods in dealing with it. In [14], [16], [31], [9]–[13], and [17], there are some typical academic papers of this type. First, in references [14] and [31], they viewed the silica as a waveguide and the Au as a defect, therefore the core mode is coupled to the defective mode in the resonance wavelength when their phases match. Consequently, the mode guided by the core will be coupled to the SP mode in the corresponding wavelength, which contributes to a loss of the core mode due to a stimulated SP mode and the absorption of the metal. The dispersion curve of the core mode can be derived based on the well-known *Kramers–Kronig (K–K)* relation. The dispersion curve of a core mode is cut off by the dispersion curve of an SP mode and it becomes two asymptotic lines of the dispersion curve of the SP mode. This deduction is correct at first sight; however, the presupposition of *K–K* relation is not sufficiently considered. *K–K* relation is deduced from the interaction of light and material. When the frequency of the inputted EM wave equals the electronic level gap, the real part and imaginary part of the RI of the material will be changed and followed by *K–K* relation. The physical explanation of this is that the material absorbs the EM wave. On the contrary, when the EM wave is guided by a waveguide and satisfies the phase condition, the wave will be coupled with the metal and will stimulate SP mode and will also be absorbed by the metal. The difference between these two different physical pictures is that the EM wave guided by a vacuum (the former) is totally absorbed by the material, but the EM wave guided by a waveguide still has a part existing in the waveguide, which will affect the absorption of the metal. Therefore, the real part and the imaginary part of the dispersion mode should not be followed by *K–K* relation. Second, in [9]–[13] and [17], they share the same viewpoint about leaky mode and defective

mode. When the phase matching condition is satisfied, the two modes will couple from high loss mode to low loss mode, but it is mandatory to utilize the concept of supermode to view a hybrid waveguide, when FEM is used to analyze the mode dispersion curves. At the phase matching point, both the core part and the defective part can guide light, causing one to be unable to extract the dispersion curves of each mode, and odd and even modes, which consist of the original core mode and the defective mode, are formed. In this regard, the dispersion curves of the modes are odd mode and even mode rather than core mode and defective mode. Finally, in [16], although we agree in form with their method of dealing with the phenomenon of anti-crossing points, their physical explanation is not comprehensive, because one curve representing two physical parameters is not reasonable. As a matter of fact, HSP mode possesses relatively low loss and thus the imaginary part of that mode can be equal to the mode guided by the silica. According to the coupled mode equation theory, when the real part and imaginary part of the refractive index of two models are equal, the original modes will be combined into two new supermodes, just as mentioned in the coupled mode explanation above.

4. Conclusion

A novel PCF SPWS based on HSP resonance has been proposed. The dispersion curves of two Au wires with equal and unequal radii aligned are investigated. Based on the derived principle of dispersion, two Au rings with unequal radii are arranged in the PCF to eliminate the unwanted polarization in the two communication windows. The coupling properties of the specific modes are investigated comprehensively by the FEM. Numerical simulations show that the proposed splitter, which is only several hundred microns in length, gives a single polarization in the two communication windows. The loss of unwanted polarization mode can reach 102.6 dB/cm and 245.0 dB/cm in the 1.31 μm and 1.55 μm wavelengths and the corresponding insertion loss is only down to 3.5 dB/cm and 1.7 dB/cm. Moreover, the dependence of the bandwidth and loss on the fiber length is derived and explained. The bandwidth and loss increase with the fiber length. According to the derived relation, the bandwidth can reach 40 nm (1.31 μm band) and 100 nm (1.55 μm band) when the fiber length is up to 1 mm and the crosstalk can reach 90 dB and 200 dB in the 1.31 μm and 1.55 μm respectively. Additionally, the tolerances for realistic fabrication are analyzed for integrity. In the last part, we discuss other methods to deal with anti-crossing phenomenon in detail.

Acknowledgment

L. Chen thanks Y. Han for discussions. Also, the authors would like to thank the anonymous reviewers for their constructive comments for the improvement of the work presented in this paper.

References

[1] N. Y. Gordeev, K. J. Gordon, and G. S. Buller, "Tunable electro-optic polarization modulator for quantum key distribution applications," *Opt. Commun.*, vol. 234, no. 1–6, pp. 203–210, Apr. 2004.
[2] J. D. Bull *et al.*, "40 Ghz electro-optic polarization modulator for fiber optic communications systems" *Proc. SPIE*, 2004, vol. 5577, pp. 133–143.
[3] [Online]. Available: http://www.generalphotonics.com/ProductDetail.aspx?dept=10&cp=57
[4] J. Martín-Regalado, J. L. A. Chilla, J. J. Rocca, and P. Brusenbach, "Polarization switching in vertical-cavity surface emitting lasers observed at constant active region temperature," *Appl. Phys. Lett.*, vol.70, no. 25, pp. 3350–3352, Apr. 1997.
[5] J. N. Caspers, J. S. Aitchison, and M. Mojahedi, "Experimental demonstration of an integrated hybrid plasmonic polarization rotator," *Opt. Lett.*, vol. 38, no. 20, pp. 4054–4057, Oct. 2013.
[6] M. F. O. Hameed and S. S. A. Obayyac, "Design of passive polarization rotator based on silica photonic crystal fiber," *Opt. Lett.*, vol. 36, no. 16, pp. 3133–3135, Aug. 2011.
[7] L. Chen *et al.*, "Passive polarization rotator based on silica photonic crystal fiber for 1.31 μm and 1.55 μm bands via adjusting the fiber length," *Chin. Phys. B.*, to be published.
[8] S. L. Jansen, I. Morita, T. C. W. Schenk, and H. Tanaka, "Long-haul transmission of 16 $\times$ 52.5 Gbits/s polarization-division multiplexed OFDM enabled by MIMO processing," *J. Opt. Netw.*, vol. 7, no. 2, pp. 173–182, Jan. 2008.

[9] S. S. Zhang, W. G. Zhang, P. C. Geng, X. L. Li, and J. Ruan, "Design of single-polarization wavelength splitter based on photonic crystal fiber," *Appl. Opt.*, vol. 5, no. 36, pp. 6576–6582, Dec. 2011.
[10] P. C. Geng *et al.*, "Orthogonal single-polarization single-core photonic crystal fiber for wavelength splitting," *Photon. Technol. Lett.*, vol. 24, no. 15, pp. 1304–1306, Aug. 2012.
[11] P. C. Geng *et al.*, "Design of broadband single-polarization single-mode photonic crystal fiber based on index-matching coupling," *Photon. Technol. Lett.*, vol. 24, no. 6, pp. 452–454, Mar. 2012.
[12] J. R. Xue *et al.*, "Polarization filter characters of the gold-coated and the liquid filled photonic crystal fiber based on surface plasmon resonance," *Opt. Exp.*, vol. 21, no. 11, pp. 13 733–13 740, Jun. 2013.
[13] Y. Du, S. G. Li, S. Liu, X. P. Zhu, and X. X. Zhang, "Polarization splitting filter characteristics of Au-filled high-birefringence photonic crystal fiber," *Appl. Phys. B*, vol. 109, no. 1, pp. 65–74, Oct. 2012.
[14] P. Li and J. L. Zhao, "Polarization-dependent coupling in gold-filled dual-core photonic crystal fibers," *Opt. Exp.*, vol. 21, no. 5, pp. 5232–5238, Mar. 2013.
[15] Y. T. Zhang *et al.*, "Microstructured fiber based plasmonic index sensor with optimized accuracy and calibration relation in large dynamic range," *Opt. Commun.*, vol. 284, no. 284, pp. 4161–4166, Aug. 2011.
[16] B. B. Shuai, L. Xia, Y. T. Zhang, and D. M. Liu, "A multi-core holey fiber based plasmonic sensor with large detection range and high linearity," *Opt. Exp.*, vol. 20, no. 6, pp. 5974–5986, Mar. 2012.
[17] B. B. Shuai, L. Xia, and D. M. Liu, "Coexistence of positive and negative refractive index sensitivity in the liquid-core photonic crystal fiber based plasmonic sensor," *Opt. Exp.*, vol. 20, no. 23, pp. 25 858–25 866, Nov. 2012.
[18] S. Das, R. Haldar, and S. K. Varshney, "Triple-core collinear and noncollinear plasmonic photonic crystal fiber couplers," *Appl. Opt.*, vol. 52, no. 34, pp. 8199–8204, Dec. 2013.
[19] W. L. Barnes, A. Dereux, and T. W. Ebbesen, "Surface plasmon subwavelength optics," *Nature*, vol. 424, no. 6950, pp. 824–830, Aug. 2003.
[20] M. Z. Alam, J. Meier, J. S. Aitchison, and M. Mojahedi, "Propagation characteristics of hybrid modes supported by metal-low-high index waveguides and bends," *Opt. Exp.*, vol. 18, no. 12, pp. 12 971–12 979, Jun. 2010.
[21] P. J. Chiang, Y. C. Chiang, N. H. Sun, and S. X. Hong, "Analysis of optical waveguides with ultra-thin metal film based on the multidomain pseudospectral frequency-domain method," *Opt. Exp.*, vol. 19, no. 5, pp. 4324–4336, Feb. 2011.
[22] L. F. Gao, Y. J. Huo, J. S. Harris, and Z. P. Zhou, "Ultra-compact and low-loss polarization rotator based on asymmetric hybrid plasmonic waveguide," *Photon. Technol. Lett.*, vol. 25, no. 21, pp. 2081–2084, Nov. 2013.
[23] H. T. Liu and P. Lalanne, "Microscopic theory of the extraordinary optical transmission," *Nature*, vol. 452, no. 7188, pp. 728–731, Apr. 2008.
[24] F. van Beijnum *et al.*, "Quasi-cylindrical wave contribution in experiments on extraordinary optical transmission," *Nature*, vol. 492, no. 7429, pp. 411–414, Dec. 2012.
[25] M. A. Schmidt and P. S. J. Russell, "Long-range spiralling surface plasmon modes on metallic nanowires," *Opt. Exp.*, vol. 16, no. 18, pp. 13 617–13 623, Sep. 2008.
[26] G. P. Agrawal, *Nonlinear Fiber Optics*. San Diego, CA, USA: Academic, 2009.
[27] A. Vial, A. S. Grimault, D. Macías, D. Barchiesi, and M. L. de la Chapelle, "Improved analytical fit of gold dispersion: Application to the modeling of extinction spectra with a finite-difference time-domain method," *Phys. Rev. B*, vol. 71, no. 8, 085416–085422, Feb. 2005.
[28] H. W. Lee, M. A. Schmidt, and P. S. J. Russell, "Excitation of a nanowire "molecule" in gold-filled photonic crystal fiber," *Opt. Lett.* vol. 37, no. 14, pp. 2946–2948, Jul. 2012.
[29] Z. H. Zhang, Y. F. Shi, B. M. Bian, and J. Lu, "Dependence of leaky mode coupling on loss in photonic crystal fiber with hybrid cladding," *Opt. Exp.*, vol. 16, no. 3, pp. 1915–1922, Feb. 2008.
[30] X. R. Ma *et al.*, "Characteristics of spectral-hole burning in Tm^{3+}: YAG based on the Perturbation Theory," *Chin. Phys. B*, vol. 23, no. 6, 060304, Jun. 2014.
[31] A. Nagasaki, K. Saitoh, and M. Koshiba, "Polarization characteristics of photonic crystal fibers selectively filled with metal wires into cladding air holes," *Opt. Exp.*, vol. 19, no. 4, pp. 3799–3808, Feb. 2011.